

# IR Temperature Measurements to Determine Fin Effectiveness of Longitudinal Fins

by A. Willockx\*, C. T'Joen\*, H.-J. Steeman\*, H. Canière\*, G. De Mey\*\*, and M. De Paepe\*

\*Department of Flow, Heat and Combustion Mechanics, Ghent University-UGENT, Gent, Belgium

\*\*Department of Electronics and Information Systems, Ghent University-UGENT, Gent, Belgium

## Abstract

The goal of this study is to determine the fin effectiveness and local convection coefficients of longitudinal fins with a coupled experimental-numerical method. Therefore the conductive heat fluxes through the cooling fin need to be known. Fin temperatures are measured experimentally with infrared thermography and these measurement data are used as boundary conditions for a 3D numerical fin model. In order to determine the heat fluxes through the cooling fin from surface temperature, an inverse heat conduction problem (IHCP) has to be solved. Results from some numerical and an experimental test case give accurate fin effectiveness, but still show significant fluctuations on the heat fluxes. The numerical IHCP algorithm still needs to be improved.

## 1. Introduction

Fins are widely used in heat exchangers, for cooling of electronics,... A good fin performance indicator is important for the design. Two potential indicators are fin efficiency and fin effectiveness. Fin efficiency is the commonly used parameter, but has the big disadvantage that the real performance of the fin is compared to the performance of an ideal non-existing fin of the same shape but with infinitely high thermal conductance. This makes it difficult to compare the thermal performance of different fin forms. Fin efficiency is an idealization and has physically no meaning. On the other hand, fin effectiveness measures the heat transfer gain obtained by placement of the fin and gives an idea of its real performance. It gives the ratio of the heat transferred by the fin to the heat transferred from the surface covered by the fin's base under the same thermal conditions, in the absence of the fin. Fin effectiveness makes it possible to compare the performance of different types of fins and thus is a better performance indicator [1]. This can be used to develop a decision system to choose a fin type in order to remove a certain amount of heat from a surface for a given free surface area.

Geometrical variations of longitudinal fins for heat transfer enhancement have previously been researched [2-4]. Matrices of flat plate fins [2], perforated fins [3] and dimpled channels [4] have been considered. However the effectiveness of these fin types is not determined. The local convective heat transfer coefficients were determined but only for specific arrangements. The matrix of the flat plate fins had a significant influence on the convective heat transfer. Unlike the test cases in this paper, the fins investigated in the mentioned papers [2-4] were exposed to a perpendicular air stream. In this paper, the air flow is parallel to the longitudinal fins.

The objective of this paper is to identify the fin effectiveness as well as the variation of the local convective heat transfer coefficient on the fin surface. Therefore the heat fluxes through the fin model and the primary surface need to be known. It is very difficult to do accurate heat flux measurements or measure a heat flux distribution on a surface, especially for large surfaces. Therefore preference is given to temperature measurements, which are more accurate and easier to perform. Complete surface temperature profiles can be measured with an infrared camera. The use of infrared thermography to measure surface temperatures from which heat flux distributions are determined is not uncommon [5,6]. Heat flux distributions [6] or convection coefficient profiles [5] can be calculated from surface temperatures by solving an inverse heat conduction problem (IHCP), which is a mathematically ill-posed problem and cannot be solved directly with CFD. There exist various solution methods for inverse heat conduction problems. The description and solution of IHCP's is highly mathematical and falls out of the scope of this paper.

In this study, a procedure is developed in which experimental measurements are coupled with an inverse numerical algorithm in order to determine fin effectiveness and local convection coefficient distribution for different fin forms. The experimental setup and measurements are described thoroughly, with special attention to the use of infrared thermography. The solution methodology of the IHCP is described, but for the detailed numerical solution method of the IHCP is referred to [7]. An example case is illustrated.

## 2. Experimental setup

### 2.1 Test rig

A test rig is designed in which both fin effectiveness and local heat transfer coefficients for different fin forms can be determined. In order to experimentally determine fin effectiveness, heat fluxes through the primary surface and the fin need to be measured. However, heat flux measurements are very delicate, have relatively large measurement errors and the heat flux distribution is disturbed by the measurement. Moreover, it is not possible with the current techniques to measure the heat flux distribution on a surface at one moment. This would require many sensors on the surface, which should influence the heat flux distribution and the air flow on the surface. Therefore it was chosen to measure temperatures and calculate heat fluxes from these measurements, which means that an IHCP needs to be solved. Thus the experimental measurements are processed by a numerical procedure to obtain the heat fluxes, so actually this is a coupled experimental-numerical study. This procedure has the advantage that the measurements are more accurate, easier and faster. The surface

temperatures are measured with an infrared camera, which has two big advantages: it gives a temperature distribution on a surface with one measurement. and it is a non-intrusive measurement technique. Air flow, temperature and heat flux distribution are not disturbed by the temperature measurement, which increases the accuracy. The biggest error in the heat flux determination depends on the accuracy of the IHCP solution, not the experimental measurements.

The definition of fin effectiveness is the ratio of heat exchange by the fin ( $=Q_f$ ) to that of the primary surface that is covered by the fin's base in absence of the fin ( $=Q_b$ ), thus:

$$\eta = \frac{Q_f}{Q_b} \quad (1)$$

So in order to experimentally determine fin effectiveness, a primary surface has to be heated and the heat flux through this surface has to be known. In a second phase, a fin is placed on a part of this heated primary surface and the heat flux through the fin is determined. The setup is built as follows. A rectangular aluminum reference block is heated at the bottom. The upper surface of the block is the primary surface. A second aluminum block of the same dimensions is made, but with an aluminum cooling fin on top. Aluminum is used because of its high thermal conductivity ( $k = 200 \text{ W/mK}$ ). A flexible isoflux heat foil is placed at the bottom of the reference block in order to induce a heat flux through the primary surface. The heat losses sideways and especially downwards need to be minimized in order to force all heat flux upwards through the aluminum block and fin. Therefore a guard heater assembly is constructed around the primary surface. The guard heater is set at the same temperature as the bottom and side walls of the aluminum block, which are measured with thermocouples. So there are almost no conduction heat losses at the bottom of the upper heat foil and from the side walls of the block due to a lack of temperature difference. The aluminum block with cooling fin and the guard heater assembly are set in a slab of polyurethane and placed in a wind tunnel with a rectangular test section (figure 1). The wind tunnel is used to examine the influence of Re-number on the local convective heat transfer coefficient and fin effectiveness. The Reynolds number (based on fin length as reference length) can be varied from 12750 to 63750. The base of the fin is at the same height as the bottom of the wind tunnel (figure 1) to avoid disturbance of the air flow at the test section. The temperature profiles on the fin surface and top of the reference block (primary surface) are measured by infrared thermography. Some adjustments were made to the test rig in order to use this measurement technique.

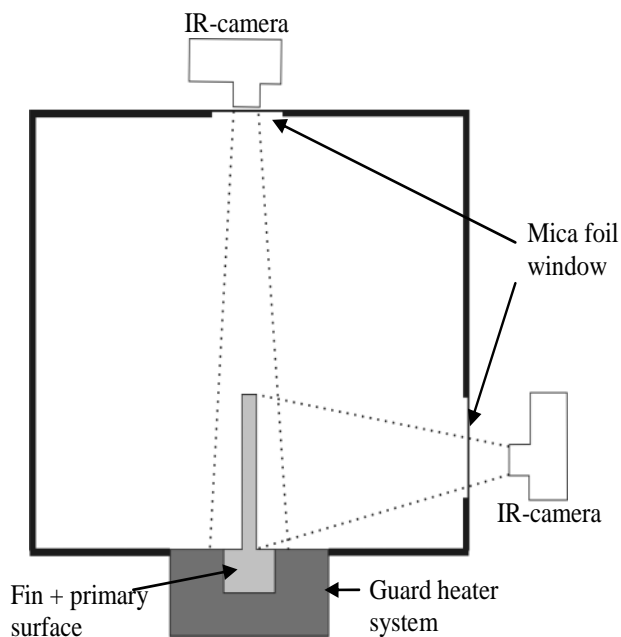


**Fig. 1:** Experimental setup in test section wind tunnel

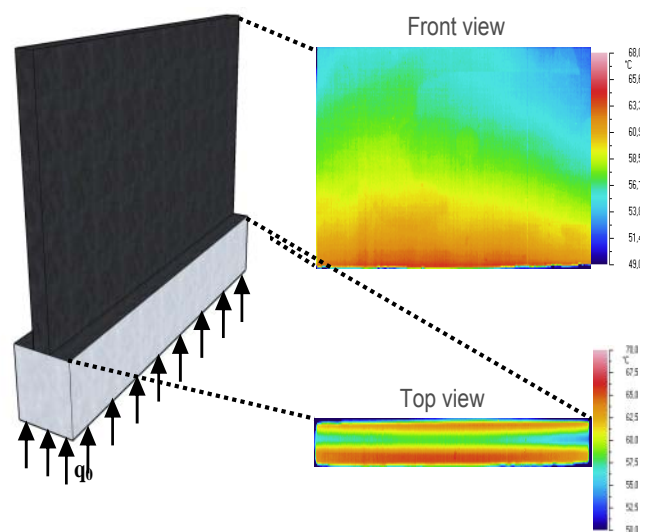


**Fig. 2:** Infrared temperature measurements

## 2.2 Infrared thermography as measurement technique

The goal of this research is to study longitudinal fins of heat sinks to cool electronics; which have dimensions of the order of magnitude of 60mm long, 40mm high and 1 mm thick. It was chosen to upscale the fin dimensions 4 times. This improves the temperature resolution, especially at the sides of the fin where there is interference with the surrounding temperatures of the colder wind tunnel wall. This influence is bigger for temperature measurements of small objects, so scaling improves the accuracy of the temperature measurement and thus on the determination of the local convection coefficient. The scaling of the fin dimensions also eases the general design of the test rig.

Thermography has the big advantage that it is a non-intrusive measurement technique and a complete temperature distribution is obtained with one measurement. However, the front and back of the wind tunnel are made out of Plexiglas. As most common solid materials, Plexiglas is not transparent for infrared radiation, which would make it impossible to measure the fin temperature with the infrared camera placed outside the wind tunnel.

Therefore infrared transparent windows are necessary. The temperature image of the front side is the same as the rear side due to the symmetry and the isoflux heat flux at the bottom of the block, so only one side of the fin needs to be measured. The temperatures at the upper side of the fin and the primary surface are also measured (figure 2). Thus two windows need to be placed: one at the top and one at the side of the wind tunnel test section (figure 1). A Midas long wave (LW) infrared camera, which has a spectral response from 8  $\mu\text{m}$  to 14  $\mu\text{m}$ , is used. Mica foil is very thin and has a relatively high transmittance for IR-radiation in the LW spectrum. Compared to most materials used for infrared transparent windows, mica is a very cheap material. Therefore both windows were made of mica foil.

An object with a high emissivity has a low reflectivity and therefore there is less influence of the surroundings on the temperature measurement. The fin and primary surface are made out of aluminum, which has a relatively low emissivity. Therefore they are painted with a matt black paint, which has a high emissivity and will increase the accuracy of the measurements.

### 3. Measurements

#### 3.1 Calibration IR-camera

The IR-camera has to be calibrated for each test case. Kirchhoff Law states:

$$\varepsilon + \rho + \tau = 1 \quad (2)$$

So three important parameters need to be calibrated in order to do accurate measurements: emissivity  $\varepsilon$  of the fin, transmittance  $\tau$  the mica foil window and the parameter:  $T_{\text{amb}}$ .  $T_{\text{amb}}$  is a measure of the mean temperature of the surroundings which becomes important in case of low emissivity and thus high reflectivity  $\rho$ . The fin and block are painted with matt black paint, which has a high emissivity. The emissivity is determined according to the ASTM Standard E 1933–99a method. Emissivity is temperature dependent and the temperatures of the fin are situated in the range from 40°C to 65°C for all measurements, so emissivity of the black paint needs to be determined for this temperature interval. A thermocouple is placed in the fin wall. First the fin is heated to a temperature of 40°C at the thermocouple position and an infrared image is taken. The emissivity of IR-camera is adjusted until the measured temperature equals the temperature given by the thermocouple. Then the fin temperature is increased with 1°C and a new image is taken and emissivity adjusted. This process is repeated till the temperature of 80°C is attained. A repetition of this test increases the accuracy. Every sequence of measurements gives an almost constant emissivity of  $\varepsilon = 0.929$  (figure3).

To calculate the transmittance  $\tau$  of the mica foil, the fin is heated until it reaches steady state. Two pictures are taken, one with the mica foil window and one without the window. The factor with which the temperature decreases by placement of the mica foil window is a measure for the transmittance of the mica foil. The transmittance of the camera is adapted until its temperature equals the temperature of the correspondent infrared picture without mica foil. The transmittance  $\tau$  of the mica foil window is determined at  $\tau=0.82$  (figure4). The sensor is also exposed to radiation which consists of various environmental contributions like radiation from the wind tunnel walls or other elements outside the wind tunnel. These factors are gathered in one parameter:  $T_{\text{amb}}$ . The influence of a small variation of this factor is negligible, mainly due to the high emissivity of the black paint.

These three parameters  $\varepsilon$ ,  $\tau$ ,  $T_{\text{amb}}$  are put in the camera as calibration values.

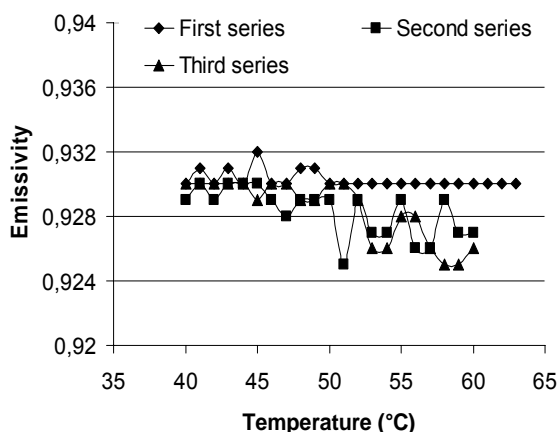


Fig. 3: Fin emissivity in function of temperature

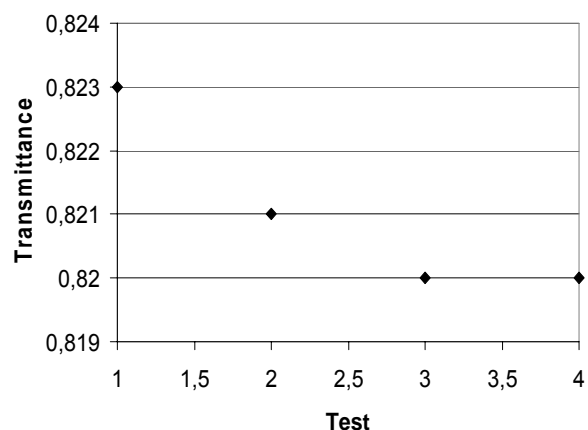
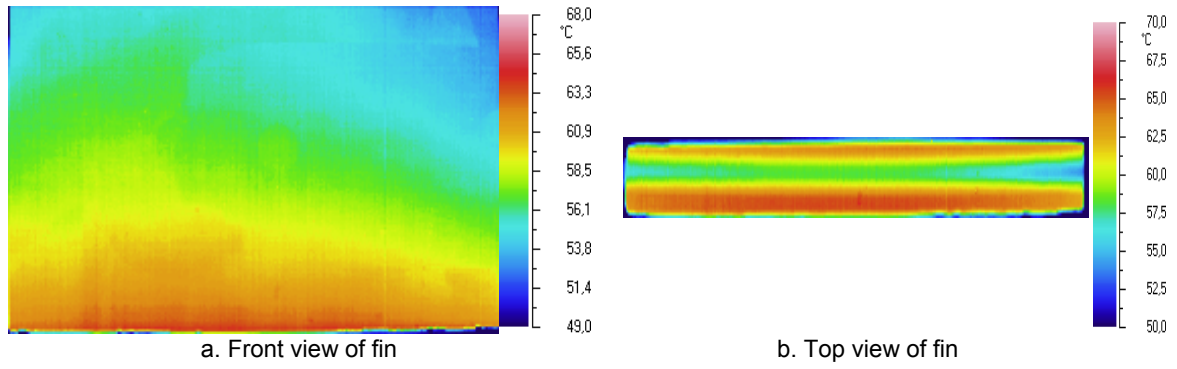


Fig. 4: Transmittance of mica foil window

#### 3.2 Measurement data

An example of the obtained temperature measurement data is shown in figure 5 for a longitudinal plate fin. In these infrared images, each pixel represents a temperature measurement.



**Fig. 5:** Infrared temperature measurement of a longitudinal plate fin

#### 4. Inverse conduction problem

These temperature measurement data are used as boundary conditions for a 3D numerical model of the fin and the primary surface (figure 6). In a direct heat conduction problem, the internal and surface temperatures of a body are determined for given boundary conditions. On the other hand, if temperature measurements are done on its boundary and the boundary conditions [6] have to be derived from these measurements, one has to solve an inverse heat conduction problem (IHCP). An IHCP is mathematically ill-posed, because the uniqueness, existence and stability of the solution cannot be assured [8]. This makes it difficult to solve an IHCP. There exist various solution methods for inverse heat conduction problems. Most methods are implemented for one or two-dimensional inverse problems [8]. The IHCP in this study is three dimensional and there is only limited literature on 3-D inverse problems, especially for determining local convection coefficients. A 3-D IHCP is difficult to solve due to the complexity and high computational cost [9].

The scaled numerical model of the fin and primary surface is shown in figure 6. The boundary conditions imposed on the fin model are inherent with those of the experiment, which gives the following three-dimensional IHCP (figure 6). The temperatures are measured on all fin surface (S1-S5) and on top of the primary surface (S6-S7). A constant heat flux  $q_0$  is induced at the bottom of the primary surface (S8) and the side walls are set adiabatic (S9-S12), which was experimentally imposed by using a guard heater. There is a thermal resistance between the primary surface and the fin, as shown in figure 6. This thermal resistance is also considered into the inverse heat conduction problem because it causes a temperature drop between the primary surface and the fin, and thus between surfaces S6-S7 and S4-S5, which could otherwise cause problems in the accuracy of the IHCP solution. The primary surface and fin are both made out of aluminium with thermal conductivity  $k=200\text{W/mK}$ .

The local convection coefficients  $h(S_i)$  on  $S_1$ - $S_7$  have to be determined, from which the heat flux distribution can also be determined. The experimental temperature measurements on these surfaces are denoted as  $Y_m(S_i)$  ( $m=1$ - $M$ ) where  $M$  is the total amount of measurement points, thus the number of pixels on the infrared image of the fin and primary surface as in figure 5. The convection coefficients  $h(S_i)$  can be estimated based on these temperature measurements  $Y_m(S_i)$ , by minimizing the functional:

$$J[h(S_i)] = \sum_{m=1}^M [T_m(S_i) - Y_m(S_i)]^2 \quad \text{for } i=1-7 \quad (3)$$

in which  $T_m(S_i)$  are the computed temperatures at the measurement locations from the direct problem solution with the estimated convection coefficients  $h(S_i)$ . A conjugate gradient method (CGM) is used to minimize the functional  $J$  in Eq. (3). The CGM is coupled with the finite volume code FLUENT [10]. However, the heat fluxes on the fin surface obtained with this numerical algorithm still show significant fluctuations which are not physical but inherent to ill-posed problems. In order to dampen these fluctuations, a first order Tikhonov regularization is added to the numerical algorithm. A detailed description of the numerical algorithm is given in [7].

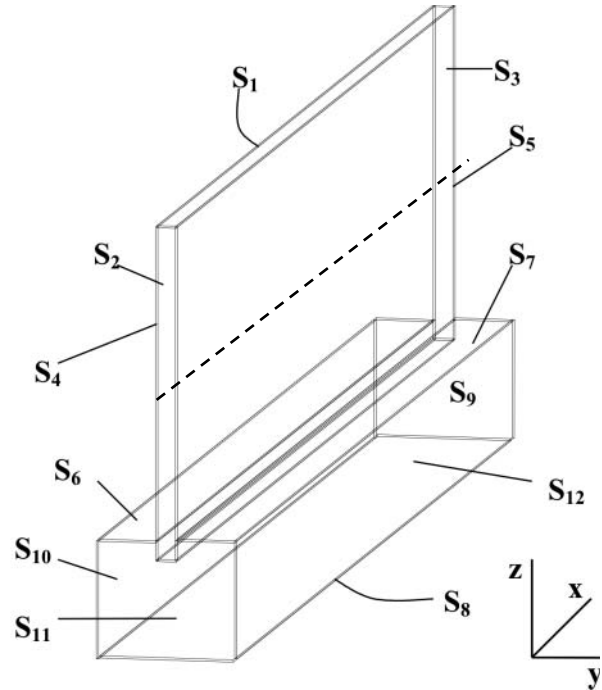


**Fig. 6:** Fin model for inverse conduction problem

## 5. Results

### 5.1 Numerical test cases

The accuracy of the numerical algorithm to solve the IHCP first has to be checked for the described model of a longitudinal fin (figure 6). Therefore some numerical test cases are developed: the temperature profiles on boundaries  $S_1$ - $S_7$  are numerically simulated by solving a direct heat conduction problem with imposed convection coefficient profiles on surfaces  $S_1$ - $S_7$ . It is assumed that there are no measurement errors on these simulated temperatures. These simulated temperatures on  $S_1$ - $S_7$  are denoted  $Y_m(S_i)$ . The grid of the fin model consists of 303057 cells. The number of cells on the fin side is equal to the number of pixels (thus measurement points) of the thermographic measurement. This means that each cell corresponds with a pixel or measurement point. On the seven surfaces  $S_1$ - $S_7$  there are 63477 measurement points (=M in Eq.(3)). This large amount of measurement points can cause long calculation times before convergence is obtained. Several test cases were simulated, two of which will be discussed

#### 5.1.1 First case: Linear convection coefficient profile

In the first case a linear convection coefficient profile is imposed on  $S_1, S_4, S_5, S_6, S_7$  over the length of the fin (x-direction in figure 3) from  $h=10\text{W/m}^2\text{K}$  at  $S_2$  till  $40\text{W/m}^2\text{K}$  at  $S_3$ . There is no change of the profile over the height of the fin. The convection coefficient profile is shown in figure 7a for the front side of the fin ( $S_5$ ) over the length of the fin (thus along x-axis) at the middle of the fin height. (dashed line in figure 6). The simulated temperatures on  $S_1$ - $S_7$  are the measured temperatures  $Y_m(S_i)$  of Eq. (3) and have to be reconstructed by solving the IHCP. The solution of the IHCP with the numerical algorithm gives the estimated convection coefficient profiles on these surfaces and is compared with the imposed convection coefficient profile. In figure 8a, the relative error between the calculated and imposed convection coefficients over the fin length of the fin at the middle of the fin height is set out. The largest error is 2.5%, so the measured and estimated temperature profiles are almost identical.

#### 5.1.2 Second case: Exponential convection coefficient profile

In this case, the convection coefficient profiles on surfaces  $S_1$ - $S_7$  are based on the boundary layer thickness for a given wind speed along the fin. Such a convection coefficient profile has an exponential form. The convection coefficient profile is shown in figure 7b for the front side of the fin ( $S_5$ ) over the length of the fin at the middle of the fin height. In figure 8b, the relative error on the estimated  $h(S_i)$  is set out.

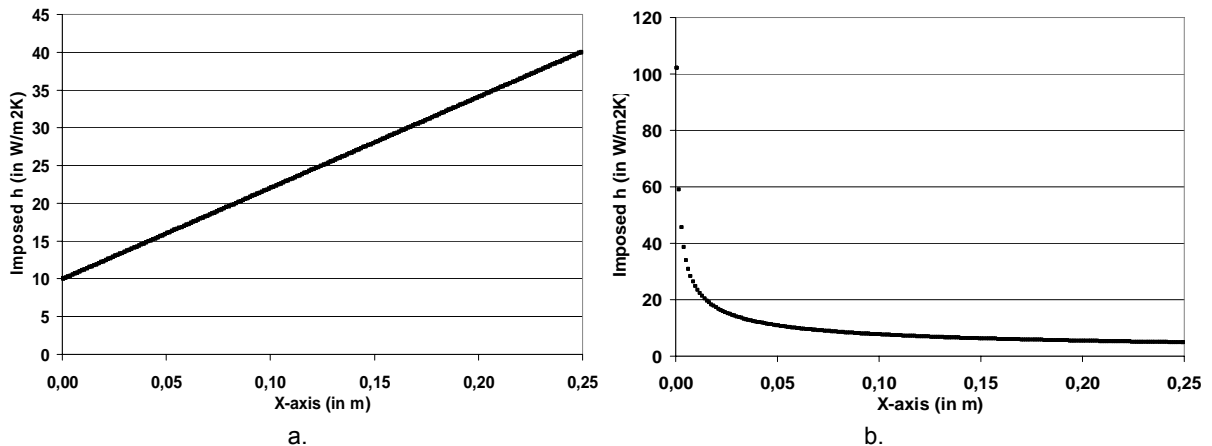


Fig 7: Imposed  $h$ -profile on the fin surface halfway the fin height: a. Linear; b. Exponential

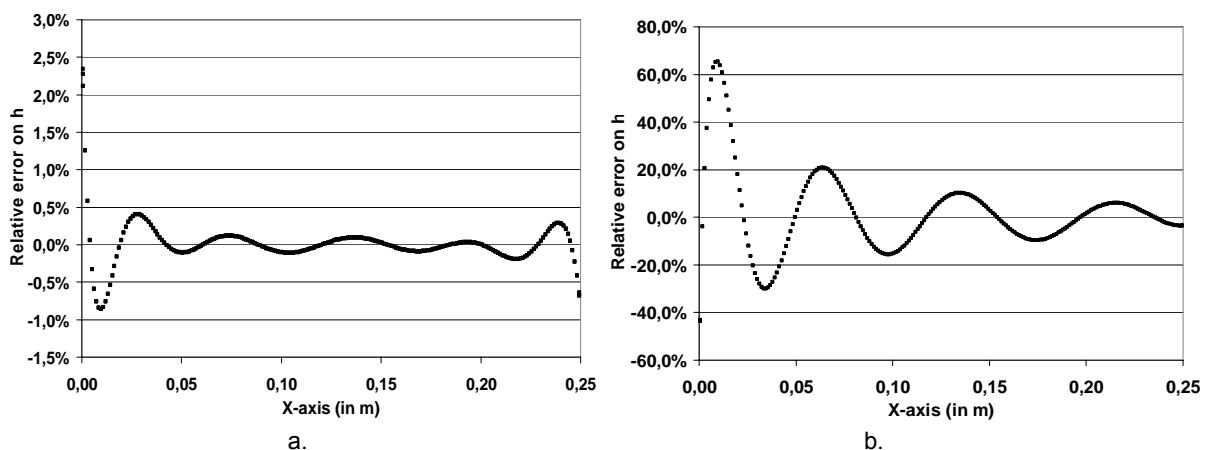


Fig 8: Relative error on solution of IHCP halfway the fin height for: a. linear  $h$ -profile; b. a. exponential  $h$ -profile

### 5.1.3 Fin effectiveness

From the solution of the IHCP it is possible to determine fin effectiveness. In Table 1, the fin effectiveness is determined with the IHCP solution and with a direct conduction calculation. The results show that the solution of the IHCP with the numerical algorithm gives accurate results for the fin effectiveness. So the IHCP algorithm can be used to determine the fin effectiveness from experimental temperature measurements.

**Table 1:** Accuracy of numerical algorithm for fin effectiveness

	Effectiveness direct conduction	Effectiveness IHCP	Error
Case a	4.580	4.580	0.0024%
Case b	4.663	4.662	0.01%

### 5.1.4 Discussion

In the first case, the J-functional of Eq.(3) drops below  $8 \cdot 10^{-5}$  after 300 iterations of the IHCP algorithm, which means a maximum error of  $3 \cdot 10^{-5}K$  on each temperature measurement. In the second case, the J-functional drops below 1.6 after 340 iterations, which corresponds with a maximum error of 0.003K on each temperature measurement. Although the obtained temperature profiles on  $S_1-S_7$  are correct, there is an error on the estimated  $h(S_i)$ . There is a wiggle in the estimated convection coefficient profile with alternating areas of positive and relative errors (Figs.7a and 7b). In the first case, these errors are small (<1%). In the second case, they become much bigger: up to 60% on the left side of the fin (figure 8b) where the imposed exponential profile has the biggest value i.e.  $100W/m^2K$ .

The big error in the second case is induced by the large  $h(S_i)$  values in these first cells at the left side of  $S_5$  and on  $S_2$ . After the first few cells,  $h(S_i)$  drops quickly to values below  $20 W/m^2K$  and remains between 15 and  $10 W/m^2K$  for the largest part of the fin. It is seen on figure 8b that  $h(S_i)$  is largely overestimated (>60%) in the first cells, followed by a larger region of underestimation (>30%), then again a zone of overestimated  $h(S_i)$  ( $\pm 20\%$ ), and finally a region of small over- and underestimation. So the relative errors decrease over the length of the fin, and the area of positive and negative relative error zones is inverse proportional with the absolute value of the error. The results of case a show that the algorithm gives better results if there is no large peak in the imposed h-profiles.

Thus it seems that the algorithm still has difficulties to capture peaks in convection coefficient profiles and still needs to be adjusted to improve the accuracy. These numerical test cases show that it is not possible yet to use the algorithm to determine the local convection coefficient profile from experimental temperature measurements. However, the calculated profiles fluctuate around the correct solution and the global flux distribution over the different temperature surfaces seems to be correct. The results in Table 1 confirm this: although the local convection coefficient profiles cannot be determined accurately, the fin effectiveness is calculated precisely (only 0.01% error). Therefore it is already possible to use the numerical IHCP algorithm to determine the fin effectiveness from the experimental temperature measurements.

## 5.2 Experimental results

Results are already obtained for the simplest longitudinal fin form: a straight rectangular longitudinal fin. It can be seen in figure 9 that there is a small drop in the fin effectiveness with increasing Re-number (2.7% drop for Re from 12500 to 62500). This drop is mainly due to measurement errors and thus the error on the fin effectiveness. So fin effectiveness remains nearly constant for varying Re in the obtained range of Re-numbers

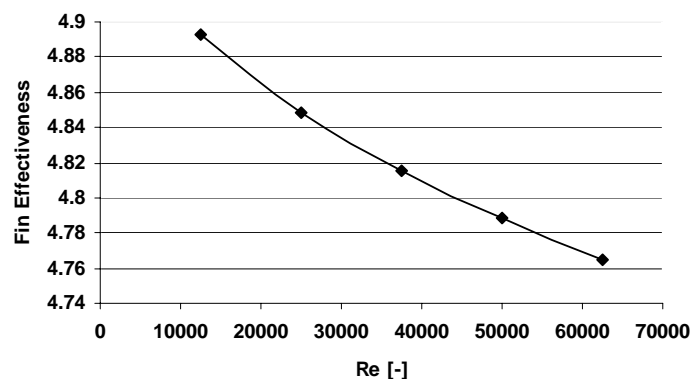


**Fig. 9:** Fin effectiveness at different Re-numbers for a straight longitudinal fin

## 6. Conclusion

A coupled experimental-numerical method is developed to determine fin effectiveness and local convection coefficients for longitudinal fins. Therefore a 3-D IHCP has to be solved. With the developed algorithm the 3D

IHCP can be solved but still lacks accuracy for the real, more complex h-profiles. This still needs to be improved. Fin effectiveness can already be determined accurately, and results are shown for a straight rectangular fin.

## REFERENCES

- [1] P.J. Heggs, Fin Effectiveness Is a Better Performance Indicator Than Fin Efficiency, *Impeche Conference Transactions*, Vol. 1999-7 (1999), 3
- [2] G. Guglielmini, E. Nannei, G. Tanda, Natural Convection and Radiation Heat Transfer From Staggered Vertical Fins, *International Journal Heat and Mass Transfer*, Vol. 30, No. 9 (1987), 1941-1948
- [3] J-M. Buchlin., Convective Heat Transfer in a Channel with Perforated Ribs, *International Journal of Thermal Sciences*, Vol. 41, No. 4 (2002) 332-340
- [4] G.I. Mahmood, P.M. Ligrani, Heat Transfer in a Dimpled Channel: Combined Influences of Aspect Ratio, Temperature Ratio, Reynolds Number and Flow Structure, *International Journal of Heat and Mass Transfer*, Vol. 45, No. 10 (2002) 2011-2020
- [5] C.H. Huang, I.C. Yuan, Ay, A three-dimensional inverse problem in imaging the local heat transfer coefficients for plate finned-tube heat exchangers, *International Journal of Heat and Mass Transfer*, Vol. 46 (2003) 3629-3638
- [6] C.H. Huang, S.P. Wang, A three-dimensional inverse heat conduction problem in estimating surface heat flux by conjugate gradient method, *International Journal of Heat and Mass Transfer*, Vol. 42 (1999) 3387-3403
- [7] A. Willockx, C. T'Joen, H-J. Steeman, H. Canière, M. De Paepe, Fin Effectiveness in Longitudinal Fins: Solving the Inverse Heat Conduction Problem, *The 19th International Symposium on Transport Phenomena, 17-20 August, 2008, Reykjavik, ICELAND*
- [8] J.V. Beck, B. Blackwell, and C.R. St. Clair jr., *Inverse Heat Conduction*, Wiley, New York (1985)
- [9] S.K. Kim, J.S. Lee, W.I. Lee, A solution method for a nonlinear three-dimensional inverse heat conduction problem using the sequential gradient method combined with cubic-spline function specification, *Numerical Heat Transfer, Part B*, Vol. 43 (2003) 43-61
- [10] FLUENT User's Guide, Version 6.1, Fluent Incorporated